Journal Pre-proof

3D printed fluidic platform with *in-situ* covalently immobilized polymer monolithic column for automatic solid-phase extraction

Enrique Javier Carrasco-Correa, David J. Cocovi-Solberg, José Manuel Herrero-Martínez, Ernesto Francisco Simó-Alfonso, Manuel Miró

PII: S0003-2670(20)30342-1

DOI: https://doi.org/10.1016/j.aca.2020.03.033

Reference: ACA 237532

To appear in: *Analytica Chimica Acta*

Received Date: 13 February 2020

Revised Date: 15 March 2020

Accepted Date: 16 March 2020

Please cite this article as: E.J. Carrasco-Correa, D.J. Cocovi-Solberg, J.M. Herrero-Martínez, E.F. Simó-Alfonso, M. Miró, 3D printed fluidic platform with *in-situ* covalently immobilized polymer monolithic column for automatic solid-phase extraction, *Analytica Chimica Acta*, https://doi.org/10.1016/j.aca.2020.03.033.

3D printed fluidic platform with *in-situ* covalently immobilized polymer monolithic column for automatic solid-phase extraction

Enrique Javier Carrasco-Correa[1*], David J. Cocovi-Solberg[2], José Manuel Herrero-Martínez[1], Ernesto Francisco Simó-Alfonso[1], Manuel Miró[2*]

[1] *University of Valencia, Spain, Department of Analytical Chemistry, University of Valencia, C/Doctor Moliner 50, 46100 Burjassot Valencia*

[2] *FI-TRACE group, Department of Chemistry, University of Balearic Islands, Carretera de Valldemossa, km 7.5, E-07122 Palma de Mallorca, Spain*

*Corresponding authors:

Dr. Enrique Javier Carrasco-Correa

e-mail: enrique.carrasco@uv.es

Tel.: +34963544062

Fax: +34963544436

Prof. Manuel Miró

e-mail: manuel.miro@uib.es

Tel: +34 971172746

Fax: +34 971173426

Abstract

In this work, 3D stereolithographic printing is proposed for the first time for the fabrication of fluidic devices aimed at *in-situ* covalent immobilization of polymer monolithic columns. Integration in advanced flow injection systems capitalized upon programmable flow was realized for fully automatic solid-phase extraction (SPE) and clean-up procedures as a 'front-end' to on-line liquid chromatography. The as-fabricated 3D-printed extraction column devices were designed to tolerate the pressure drop of forward-flow fluidic systems when handling large sample volumes as demonstrated by the determination of anti-microbial agents, and plastic additives and monomers as models of emerging contaminants (4-hydroxybenzoic acid, methylparaben, phenylparaben, bisphenol A and triclosan). Decoration of the monolithic phase with gold nanoparticles (AuNPs) was proven most appropriate for the enrichment of phenolic-type target compounds. In particular, the absolute recoveries for the tested analytes ranged from 73-92% both in water and saliva samples. The 3D printed composite monolith showed remarkable analytical features in terms of loading capacity (2 mg g^{-1}), breakthrough volume (10 mL), satisfactory batch-to-batch reproducibility (<9% RSD), and easy on-line coupling of the SPE device to HPLC systems. The fully automatic 3D-printed SPE-HPLC hyphenated system was also exploited for the on-line extraction, matrix clean-up and determination of triclosan in 200 µL of real saliva samples.

1. INTRODUCTION

Porous organic monolithic materials are attractive stationary phases for separation and sample preparation in analytical science owing to their good permeability, easy preparation and chemical modification[1,2]. However, due to the small surface area of the porous monoliths, their combination with high surface-to-volume ratio (nano)materials (namely, metallic nanomaterials, metallic organic frameworks, carbon nanostructures, etc.) opened up new opportunities for the separation and/or enrichment of small molecules in a variety of samples[1,3–5]. Particularly, the use of gold nanoparticles (AuNPs) poses several advantages because of: (i) the stability of the NPs, (ii) the specific interactions with sulphur moieties and amine derivatives[6], and (iii) the easy monolith-surface attachment[7]. Several research groups have described appealing solid-phase extraction (SPE)-based methodologies using AuNP-decorated monoliths for proteins[7,8], oligopeptides[9], and thiol-containing compounds[10].

Another interesting feature of porous organic monoliths is that they can be prepared *in situ* within the confines of a mold, thus allowing synthesis to be effected in practically any tailorable support (viz., metallic columns, silica capillaries, disks, spin columns, pipette tips and cartridges). However, polymer monoliths are usually milled, sieved and packed within frits thus resembling conventional SPE columns[7,8,11]. Polymer monoliths can be advantageously employed in on-line sample preparation methods, such as on-line SPE, and solid-phase microextraction (SPME)[3], because of minimum pressure drop, as compared to particle columns which tend to pack progressively tighter in on-line fluidic systems[12]. However, on-line methodologies reported so far using monolithic structures have been capitalized on *in-tube* [13] or microchip formats[14,15], which suffer from rigid architectures, and/or lack of unsupervised operation. In addition, *in-tube* silica capillaries or microchips containing monolithic phases are inappropriate for extraction and preconcentration protocols because of the limited sample volume that can be loaded. Also, chip-based devices usually incorporated

physically constrained polymer organic monoliths rather than covalently attached stationary phases [16]. In this context, consumer-grade 3D-printersthat can ideally fabricate almost any imaginable fluidic structure with a wide range of diameters might trigger a host of prospects for on-line (μ)SPE using monolithic phases.

Additive manufacturing, so-called 3D-printing, is an enabling technology for the fast prototyping of novel 3D-printed holders or supports, intricate platforms, or fluidic devices in a variety of research areas[17–24]. 3D-printing is based on a material being added layer-by-layer, which affords the design and building of structures that cannot be easily prepared by conventional subtractive methodologies[17,19,20,24]. Several cost-effective 3D printing techniques using desktop printers have been launched in the last years, including those based on fused deposition modelling (FDM) and stereolitography (SLA). Interested readers are referred to the following comprehensive reviews for a detailed description of the underlying principles of FDM, SLA and other 3D printing technologies[17–21]. In the field of sample preparation and separation science, 3D printed fluidic structures have been scarcely studied[17,20,25–27] because of the limited capacity of 3D-printed fluidic platforms with cross-sectional features at the micro or milli-dimensional scale to accommodate sorptive material with sufficient surface/exchange area. Several authors have attempted to fabricate intricate printed structures in which the pristine inner surface of 3D-printed fluidic channels or after grafting with proper ligands is exploited for size-based, ion-exchange or chelating-based separation of the target analytes[28–31]. An attractive alternative is to combine porous organic monolithic stationary phases with 3D-printed devices. Up to the date, only two research groups contemplated this possibility[16,32,33]. One of the groups at Brigham Young University developed a fluidic platform containing glycidyl methacrylate (GMA)-based monoliths for immunoaffinity extraction by using a custom 3D printer that admits polyethylene glycol diacrylate resin[16]. However, the authors did not attach the monolith to the inner surface of the channels and thus, the column might be shrunk or swelled in the time course of

the extraction, or even pushed away from the channel when increasing the linear velocity. In fact, only vacuum-assisted fluidic control was demonstrated by the authors. Also, the use of non-commercial resins led to devices that could not be readily printed by consumer-grade 3D-printers. The second group at the University of Tasmania[32,33] anchored monolithic stationary phases to titanium alloy chromatographic columns that were 3D printed by selective laser melting. In this case, the inner surface was modified with 3-trimethoxysilylpropyl methacrylate for further *in-situ* polymerization of a butyl methacrylate monolithic material. However, the use of silane-based coupling reagents could lead to hydrolysis in strong acidic/alkaline media conditions, or even in milder conditions. In addition, the effectiveness of organosilane reactions on metallic surfaces, such as titanium, is smaller compared to other materials like silica, quartz or glass that are commonly used for the covalent attachment of organic monolithic structures[34]. It should be also added that laser sintering is a costly 3D printing technology that usually leads to non-homogeneous inner surfaces that could in turn jeopardize the column reproducibility and, thus, the reliability of the separation process. Therefore, there is a quest of developing novel strategies for the reliable preparation of *in situ* porous organic monoliths covalently attached to 3D-printed devices for micro and milli-scale sorptive extraction by using commercially available technologies at low cost.

This work reports for the first time the exploration of a variety of synthetic routes for covalent attachment of porous polymers to the inner surface of acrylate-based photopolymerized resins in 3D-SLA printed fluidic platforms aimed at on-line sorptive extraction. The proof-of-concept applicability of the novel monolithic phase containing fluidic devices to which AuNPs were incorporated was demonstrated by the automatic SPE of alkyl esters of 4-hydroxybenzoic acid, bisphenol A and triclosan (used as preservatives, anti-microbials or plastic monomers in consumer products) in human saliva as a 'front-end' to on-line liquid chromatographic separations. The idea behind is to illustrate the opportunities of the recently launched 4th generation of flow injection analysis, so-called 3D-µFIA[27] in the analytical separation arena.

2. EXPERIMENTAL SECTION

Description of (i) the high-performance liquid chromatographic system, (ii) reagents and chemicals, and (iii) samples is available as Supporting Information (SI). The fabrication of the 3D-printed devices, their chemical functionalization and integration into the fluidic device is described below.

2.1. Fabrication of the 3D-printed fluidic device

The fluidic device (Fig. S1) was designed in 123D Design software (Autodesk, San Rafael, CA, USA). Despite the aim of the current contribution is to demonstrate the feasibility of covalently binding of the monolithic SPE sorbent to the inner surface of 3D printed stereolithographic fluidic objects, the design of a customized flow channel and the connections thereof to other fluidic components was also explored. The main channel has a 2 mm i.d. and a length of 50 mm (volume of ca. 157 µL) and ended with U-shaped protruding channels of 1.8 mm i.d. and 2 mm-bending radius (see Fig. S1). Two empty cylinders of 5.5 mm i.d. and 8 mm length each were appended at the ends of the channels to serve as tapper guides for the connectors in the post-printing process. The resulting U-shaped object served two-fold purposes: on one hand, it enabled the one-step fabrication of the device onto the printer platform, which implies less resin consumption along with the draining of the remnants of the liquid polymer during the printing process so as to prevent the clogging of the channel. Further, the narrowing of the channel at both ends of the device served minimize void volumes because of the potential polymer shrinking throughout the polymerization process. The overall size of the unit was 65.5 mm long, 9.5 mm wide and 16 mm high.

The 3D model was then loaded into the manufacturer's CAM software (Preform, Formlabs) for fabrication of replicates, positioning of the objects, and slicing prior to submitting the STL. file to the Form 2 printer (Formlabs, Somerville, USA). The units were printed at a nominal resolution of 50 µm (316 layers as a trade-off between speed and resolution of the final print)[25] using the FLGPCL02 (Formlabs) clear resin, without supports and with the connections facing downwards.

After retrieving the 3D printed devices from the moving platform, the devices were soaked in isopropyl alcohol (IPA) for 10 min to remove the non-polymerized resin with further perfusion of the internal channels with IPA to eliminate remnants of liquid resin. The fluidic supports were UV-cured for 24 h under a 16 W low pressure mercury lamp UV oven (KA-9180, PSKY, China) according to previous studies[22] to harden the polymerized resin and prevent unspecific leaching of non-polymerized oligomers. Once the post-printing process was finished, both connectors were manually tapered to ¼'' - 28 threads.

2.2. Modification of the inner surface of the 3D printed device

Several wet chemical procedures[35–38] were assayed for functionalization of the surface of the inner walls of the 3D-printed fluidic devices. Only the optimal procedure is described herein while the other alternative synthetic routes are available to interested readers in the SI. The optimal procedure (Fig. 1) is based on the incorporation of methacryloyl moieties onto the inner surfaces of the 3D prints for further *in-situ* polymerization. For this purpose, first, the channel of the 3D printed fluidic device is entirely filled with a 2 mol L^{-1} NaOH solution at 45 ºC for 24 h to hydrolyze the methacrylate moieties from the photopolymerized resin (step A, Fig. 1). Then, the 3D-printed object is washed subsequently with water, 0.1 mol L^{-1} HCl and IPA before drying with a N_2 steam. In the second step, the carboxylic groups generated in the interior of the channel are allowed to react with a solution containing 0.2 mol L^{-1} (1-ethyl-3-(3-dimethylaminopropyl)carbodiimide (EDC) and 0.3 mol L^{-1} N-hydroxysuccinimide (NHS) in water

for 1 h at 37 ºC (step B, Fig. 1). The 3D-printed fluidic support is subsequently washed with water and IPA, and dried with N_2. The third step consists of exchanging the NHS moieties with hexamethylendiamine (HMD) groups. The amidation reaction is achieved by filling the fluidic system with a 0.52 mol L^{-1} HMD solution in water for 2 h at 37 ºC (step C, Fig. 1). Subsequently, the channel is rinsed with water and IPA, and dried with N_2 before the last reaction. To this end, the 3D-printed channel is filled with a solution of 2 mol L^{-1} glycidyl methacrylate (GMA) in ACN and the reaction is performed for 2 h at 60 ºC (step D, Fig. 1). Prior to the polymerization step, the functionalized 3D-printed devices are washed subsequently with ACN and IPA, and dried with a N_2 steam pending use.

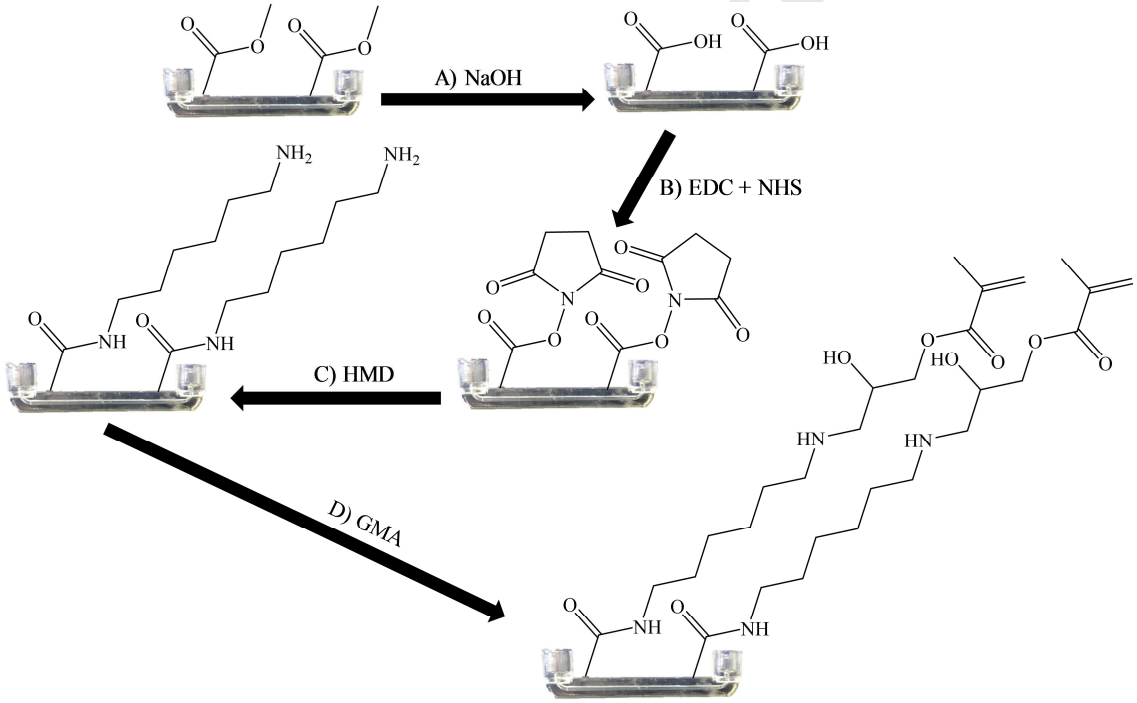

Fig. 1. Scheme of the sequential chemical modifications of the inner surface of acrylate-based 3D-prints prior to *in-situ* monolith preparation. The reagents used for the modification of the inner surface of the 3D printed support are: EDC: 1-Ethyl-3-(3-dimethylaminopropyl)carbodiimide; NHS: N-hydrosuccinimide ;HMD: hexamethylenediamine and GMA: glycidyl methacrylate.

2.3. In-situ monolithic column preparation

In-situ fabrication of the organic monolithic phase incorporated 3D-printed fluidic platform is performed by UV-polymerization following a previous report with minor changes[39]. Briefly, 220 µL of a polymerization mixture containing GMA as functional monomer (20 wt%), ethylene glycol dimethacrylate (EDMA, 5 wt%) as crosslinker, cyclohexanol (70 wt%) and 1-dodecanol (5 wt%) as porogens and 2,2-dimetoxyacetophenone (DMPA) as initiator (1 wt% with respect to the monomers) is introduced into the 3D-printed millifluidic channel to fabricate a *ca.* 50 mm-long monolithic column. UV-polymerization was performed in a 16 W low pressure Hg lamp UV oven (KA-9180, PSKY, China) for 16 h. The 3D-printed devices containing the covalently attached monoliths are flushed with IPA prior to further chemical modification. The decoration of the polymer monoliths with AuNPs is accomplished by activating the monolithic epoxy surface with 4.5 mol L^{-1} ammonia at 60 ºC for 2 h[7]. Then, the column is flushed with water until neutral pH before pumping a dispersion of 20 nm AuNPs in citrate buffer through the monolith until the entire monolithic column acquired the characteristic red-garnet color that is indicative of the attachment of AuNPs to the nitrogen moieties. Finally, the column is flushed with IPA and kept closed until use.

2.4. Fluidic Setup

A Cavro Xcalibur syringe pump (Tecan, Männeford, Switzerland) equipped with a 1 mL-glass barreled syringe and a 9-position ceramic head valve served as the microflow analysis platform integrating the 3D printed device. Fig. 2 schematically shows the flow setup for on-line microextraction as a front end to liquid chromatographic separation. The ports of the valve are used for air (port #1), deionized water (port #3), 0.1% acetic acid in water (port #4), ACN (port #7), waste (port #9), the AuNP-monolith incorporated millifluidic 3D-printed device (port #2) and the AIM3200 autosampler (Aim Lab Automation Technologies, Victoria, Australia) in port #5. As illustrated in Fig. 2, the millifluidic device is allied to a high pressure HPLC 6-port injection valve that allowed the trapping of the eluate plug from the previous SPE protocol into

the valve loop. All the tube connections are made of fluorinated ethylene propylene tubing with 1/32" i.d., except the HPLC injection loop (50 µL) which is made of PEEK tube of 1/32" i.d. The syringe pump and the autosampler are computer-controlled via the freeware automation suite Cocosoft 4.4[40]. The selection of the valve ports and the autosampler positions, the direction and speed of the syringe pump, and the synchronization of the fluidic setup with the operation of the HPLC setup for unattended analyses are performed by Cocosoft through USB-RS232 adapters (Parallax). The flow method and the HPLC operational procedure for automatic sorptive extraction and HPLC separation of the target species are listed in Tables S1 and S2, respectively.

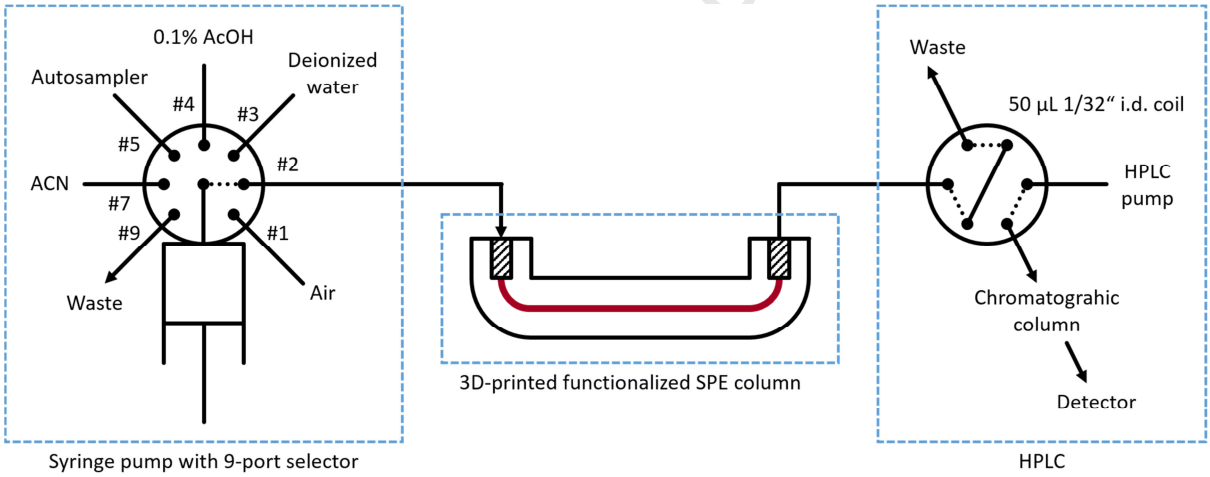

Fig. 2. Scheme of the flow setup integrating the 3D printed AuNP-decorated covalently immobilized monolithic structure as a front-end to HPLC separations.

2.5. Automatic analytical procedure

The analytical procedure consists of several standard steps of an SPE protocol that are performed unsupervised by software control by (i) selecting the port of the multi-position head valve, (ii) aspirating the appropriate amount of reagent or sample, and (iii) perfusing the solutions through the monolith by flow reversal. All volumes are aspirated and dispensed at a flow rate of 500 µL min^{-1} except those of the loading, drying and eluting steps from and to the

monolith that are dispensed at 200 µL min^{-1}. The monolith is initially conditioned with 200 µL of ACN and 500 µL of 0.1% acetic acid (HAc) followed by drying with 1000 µL of air. Then, a volume of sample ranging from 200 µL to 10,000 µL in 0.1 % HAc is perfused through the monolith with a subsequent washing step with 200 µL of 0.1% HAc and 500 µL of air. The analytes are eluted with 50 µL of ACN and the eluate is parked in the HPLC injection coil in an air-segmented manner by using 200 µL of air at the trailing edge. The pumping volume toward the HPLC valve is optimized from 150 to 250 µL by successive injections until monitoring the maximum peak area of the eluate without appreciable artifact signals attributable to air. This method is applied to all standards and samples in triplicate. The entire fluidic method including other steps such as syringe cleaning and reservoir priming lasts 11.5 min for 200 µL, and is available in Table S1. For offline detection, all the steps are the same except for the elution. In this case, the elution is performed by two steps of 200 µL ACN and collected in two different HPLC vials prior to injection (20 µL) into the HPLC system. Because the HPLC run exceeded the sample preparation method by only 1.5 min (13 min vs. 11.5 min, respectively), a very simple and straightforward strategy for unsupervised synchronization of both systems is employed[25,41] as described in SI.

3. RESULTS AND DISCUSSION

3.1. Chemical derivatization of the inner surface of 3D printed stereolithographic devices

The chemical modification of the inner surface of micro/millifluidic structures for separation purposes is an important step to endow them with the required terminated functional groups for target species. In this work, the 3D-printed SLA platform was modified by wet chemical method to incorporate pendant vinyl groups. First, the chemical structure of the commercial Clear Resin (FLGPCL02, Formlabs) was characterized by ATR-FTIR (Fig. S3A). The ATR-FTIR spectrum shows the characteristic absorption bands of a polymerized acrylate: C-O (1052 and 1141 cm^{-1}) and C=O stretches (1240 and 1701 cm^{-1}), and symmetric and asymmetric

deformations of CH_2 and CH_3 (2800-3000 cm^{-1}). The O-H stretch band (3370 cm^{-1}) can be assigned to the residual IPA used for cleaning the 3D-printed devices. Aiming at incorporating vinyl groups to the inner surface of the prints, several multi-step reactions were tested (see SI), although the only one described below allowed subsequent covalent attachment of the polymer monolith to the inner surface (see experimental section and Fig. 1). All reaction steps used along this work were monitored by ATR-FTIR (Figs. S3B-D). The first step consisted of the hydrolysis of the ester groups of the parent carboxylic acid by introducing an aqueous NaOH solution into the 3D-printed device channel (step A, Fig. 1) for 24 h at 45 ºC. The ATR-FTIR (Fig. S3B) spectra shows the band at 1702 cm^{-1} of the parent material (Fig. S3A) split into two overlapped bands at 1702 and 1694 cm^{-1} corresponding to the C=O stretches of the ester and carboxylic groups, respectively. Also, the magnitude of the O-H band (3300-3400 cm^{-1}) increased by *ca.* 30 % after the reaction due to the incorporation of O-H groups from the hydrolysis of the ester (see Fig. S3B). Then, the introduction of an alkyl diamine (e.g., HMD) is performed to obtain pendant amine moieties (see Fig. 1 C) that can subsequently react with the epoxide of the GMA. For this purpose, a two-step procedure based on the EDC-NHS coupling of primary amines to carboxylic groups (see Fig. 1B) was undertaken. However, the coupling reaction has to be carried out relatively fast because the reactive ester with EDC is rapidly hydrolyzed. First, a mixture containing EDC and NHS was introduced into the 3D-printed device for 1 h at 37 ºC (step B, Fig. 1). After washing with water and drying with a nitrogen steam, the HMD solution was pumped into the fluidic structure for chemical derivatization, thus obtaining the desired primary amine group (step C, Fig. 1). This reaction was again monitored by ATR-FTIR (Fig. S3C): The band of the C=O split in several bands corresponding to the different carbonyl groups available after the reaction, viz., amide (1722 cm^{-1}), acid (1694 cm^{-1}) and ester (1703 cm^{-1}) moieties. Also, three bands corresponding to the terminated primary amine and amide groups were found at 950 cm^{-1} (N-H bending), 1450 cm^{-1} and 1548 cm^{-1} (C-N stretch) and 3372 cm^{-1} (N-H stretch).

The last reaction step involved the introduction of GMA to generate vinyl groups anchored to the inner surface of the 3D printed device. For this purpose, the 3D printed millifluidic channel is filled with 2 mol L^{-1} GMA in ACN for 2 h at 60 ºC. The ATR-FTIR spectra (Fig. S3D) shows less bands overlapped near the C=O zone, probably due to the increase of the number of ester groups from GMA. Also, the appearance of new C=C bands (1640-1680 cm^{-1}) demonstrates the success of the last derivatization reaction. In our case, each primary amine seems to react with two GMA molecules to generate tertiary amines with two vinyl groups each. This assumption is confirmed by the decrease of the N-H bending band at 950 cm^{-1}, and the increase of a band at 1028 cm^{-1} (C-N stretching of the tertiary amine). After this procedure, as described in detail in SI (section 1.5-Preparation and characterization of the monolithic columns), the inner surface of the 3D-printed millifluidic device incorporated pendant vinyl groups that foster the anchorage by UV-copolymerization of the monomer and crosslinker (poly(GMA-*co*-EDMA)) and the modified wall inside the 3D printed object. In order to corroborate the successful covalent attachment of the monolith within the printed device, SEM micrographs of the cross-sections of the poly(GMA-*co*-EDMA) monolith (See SI and Fig S4 for the preparation and AuNP decoration of the polymer monolith) were taken. As shown in Fig. 3A, no significant voids between the inner surface and the polymeric monolith were evidenced, which confirmed that the material was tightly attached to the inner wall of the 3D-printed fluidic device. In addition, the pressure-driven flow (up to 5 mL min^{-1}) generated by the micro-syringe pump did not jeopardize the stability of the anchored phase.

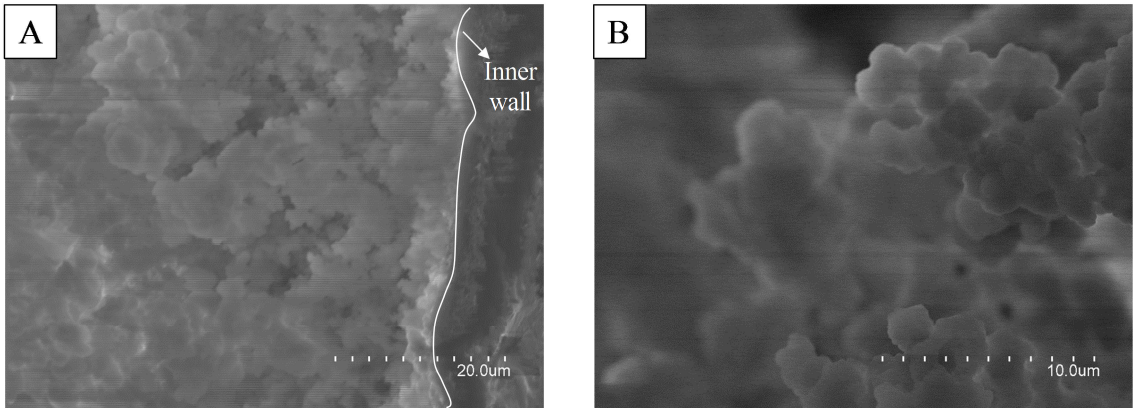

Fig. 3. SEM micrographs of the organic monolithic covalently attached to 3D-printed fluidic devices. SEM micrograph at 2000 × of the parent monolithic material at the wall zone (A) and parent monolithic morphology at 5000 × (B).

In the following experiments with on-line and off-line detection, two types of 3D-printed millifluidic devices were fabricated based on the modification of the organic monolith. The first is obtained by modification of the parent poly(GMA-*co*-EDMA) monolith with amino groups by opening of the available epoxy groups[42] with ammonia (see Experimental Section) The second is fabricated bythe immobilization of citrate-modified AuNPs[7] onto the previous device. The mechanism of the retention of the AuNPs onto amino modified surfaces is based on the complex interplay between donor-acceptor and electrostatic interactions. First, the citrate shell favors the electrostatic interactions of AuNPs with the surface amine groups. However, the main interaction is most likely due to the labile character of the citrate layer that fosters the direct bonding of the Au to the amine moieties [43].

3.2. Automatic SPE exploiting the in-situ prepared monolithic 3D-printed fluidic devices

Using flow-injection analysis, the various 3D-printed millifluidic devices described above (empty, parent, amino- and AuNP-modified monolithic sorbents) were examined for the extraction capacity of several antimicrobials and plastic additives that are currently regarded organic emerging contaminants (viz., 4-hydroxy benzoic acid, 4-HBA, methyl paraben, MPB, bisphenol A, BPA, phenyl paraben, PhPB and triclosan, TCS). The automatic SPE procedure is described in the experimental section in detail, yet off-line detection was used here for the sake of simplicity. Briefly, 200 µL of a solution containing 1 mg L^{-1} compounds in 0.1% HAc was passed through the columns, washed with 200 µL of aqueous 0.1% HAc, followed by two elution steps of 200 µL of acetonitrile. Next, 20 µL of the collected eluates were injected into the HPLC. According to Fig. 4, the empty millifluidic device showed the lowest retention

efficiency (<50%) for all the analytes as it might be expected from an *in-tube* SPE phase consisting of an empty 2 mm ID photopolymerized channel (ca. 314 mm^2). On the other hand, all the millifluidic devices containing covalently immobilized monolithic sorbents featured good retention efficiencies (>60%), yet, improved retention capacities were detected for the 3D-printed millifluidic devices containing the NH_2-modified and the AuNP-decorated monoliths (>67 and 76%, respectively). The most polar analyte, 4-HBA, showed a significant improvement in the retention by the AuNP-laden sorbent compared to the parent monolith (see Fig. 4). This behavior can be explained by the donor-acceptor interactions between the hydroxyl groups and aryl rings of the target compounds and the AuNPs[43–46], and the increase of the surface area of the monolith due to the surface attached nanoparticles[7].

The feasibility for eluting the analytes was also examined for the four distinct sorptive materials (Fig. 4). The experimental results revealed that the AuNP incorporated monolithic phase featured improved absolute recoveries (72-92% against the overall mass loaded) compared to the amino-modified (10-60%), parent monolith (35-67%) and the empty millifluidic device (0-40%). Experimental measurements of the washing solution also evidenced that the percentage of analytes eluted in the washing step of the AuNP-modified sorbent was <5% as compared to 5-25% for the parent monolith or 2-15% for the NH_2-modified monolith. In the case of the AuNP-modified column, the first elution step with 200 µL was sufficient to elute between 70 and 80% of the loaded analytes.

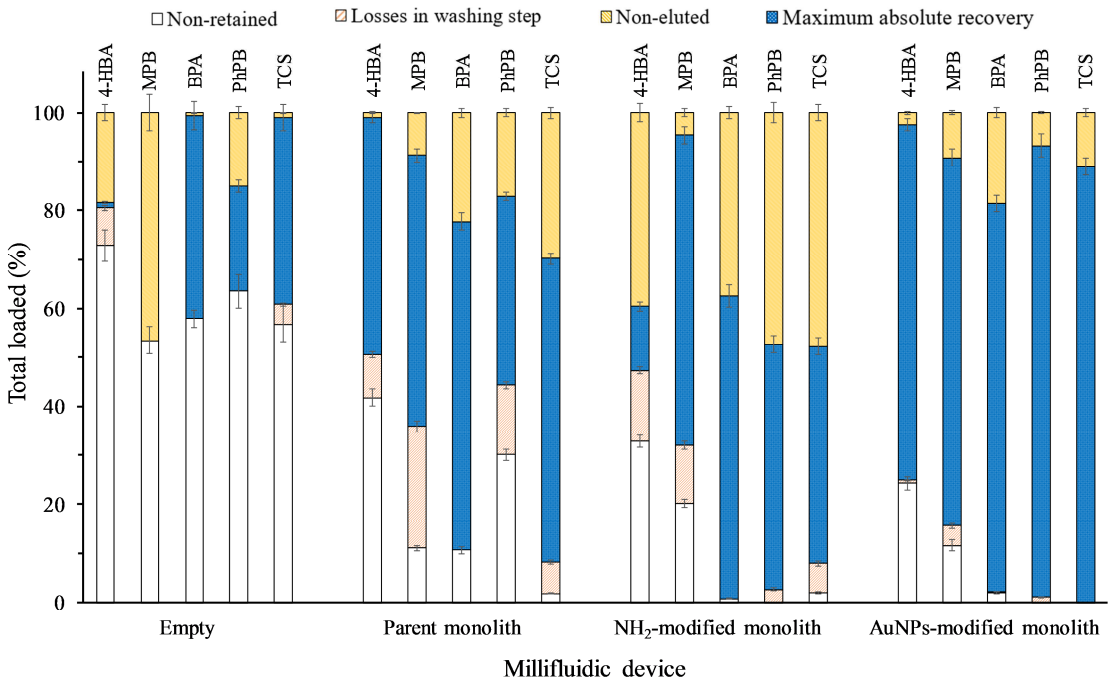

353

354 **Fig. 4.** Breakdown of the loaded mass of target analytes onto the different monolithic phases
355 attached to the 3D-printed millifluidic devices for automatic SPE. The maximum absolute
356 recovery was achieved for a total elution volume of 400 µL with off-line detection. Error bars
357 are given as SD values for three extractions performed with the same 3D-printed device.

358

359 **3.3. Analytical performance**

360 Two primary influent parameters in the automatic SPE process are: (i) the breakthrough
361 volume and (ii) the sorbent loading capacity (see Figs. S5 and S6). As observed in Fig. S5, the
362 retention efficiencies of the parent monolith dropped quickly from 58-98% down to 40-90%
363 when the loading sample volume increased from 0.2 to 1 mL. An additional decrease (down to
364 ca. 10-60%) is observed at greater loading volumes (10 mL). Similar results were encountered
365 for the amino-terminated monoliths, in which the retention efficiency also decreased rapidly.
366 On the other hand, the monolith decorated with AuNPs featured good sorptive efficiencies for
367 the suite of compounds (70-98%) even at loading volumes as large as 10 mL. With respect to
368 the loading capacity for the several 3D-printed millifluidic devices containing monolithic
369 phases (Fig. S6), the parent and the amino-modified phase showed a significant deterioration

of the retention efficiencies (down to 50-70%) even at low loadings (0.2 mg analyte per g of sorbent) of the less retained analytes. However, the 3D-printed millifluidic device with the anchored AuNPs exhibited excellent extraction efficiencies (70-97%) even for loading amounts up to 2 mg g^{-1} sorbent. These results are in agreement with previous results of organic monoliths functionalized with AuNPs for which larger analyte breakthrough volumes and improved loading capacities were observed for small compounds and biomolecules as compared with pristine monoliths[10,47,48]. Therefore, the 3D-printed devices with monolithic structures modified with AuNPs were selected for further studies.

The proposed automatic SPE protocol was validated in terms of sensitivity, linearity, precision, enrichment factors, reusability and limit of detection and quantification. A good linearity (R>0.999) was obtained for the five analytes (within the following concentration ranges: 6-2000 ng mL^{-1} for 4-HBA, MPB, BPA and PhPB, respectively, and 20-2000 ng mL^{-1} for TCS) for a sample volume of 0.2 mL with sensitivities (slopes of calibration curves) of 5,800; 4,100; 3,100; 2,400; and 5,800 mV L mg^{-1}, respectively. As shown in Table 1, satisfactory relative standard deviation (RSD) values (below 9%) for intra- and inter-3D-printed devices containing AuNP-modified monoliths were obtained for all the analytes. The limits of detection (LOD) and quantification (LOQ) of the automatic SPE protocol in acidified Milli-Q water were estimated from a signal-to-noise ratio of 3 and 10, respectively (see Table 1) The LODs obtained were better than those previously reported for the same analytes using 3D-printed millifluidic devices incorporating magnetically retained sorptive nanoparticles[25]. The enrichment factors, calculated for a 200 µL loading volume at the 1 µg mL^{-1} using the absolute recoveries in acidified Milli-Q water (see Table 2), were 2.9, 3.0, 3.2, 3.7 and 3.6 for 4-HBA, MPB, BPA, PhPB and TCS, respectively. Nevertheless, the enrichment factors at the maximum loading volume admitted (10 mL) might be increased up to 145, 150, 158, 184 and 177 for 4-HBA, MPB, BPA, PhPB and TCS, respectively. The 3D-printed monolith incorporated millifluidic

device might be reused for at least 25 injections with a change down to 7% of the absolute recoveries for all the analytes.

3.4. Sample analysis

The 3D-printed millifluidic platform with the covalently-immobilized AuNP-monolith was applied to the clean-up, extraction and preconcentration of the target species (4-HBA, MPB, BPA, PhPB and TCS) in human saliva (see SI for the detailed procedure for analysis of human saliva). An analyte-free blank saliva was spiked with 250 μg L^{-1} of each of the five analytes. The automatic SPE results for the analysis of 200 μL saliva with on-line detection were compared against those obtained by on-line processing of acidified Milli-Q water (pH=3.3) spiked at the same concentration level. The absolute recoveries calculated against external mass calibration with aqueous standards ranged from 71-89% for the saliva samples and 73-92% for Milli-Q water (see Table 2). The *t*-test of comparison of means revealed that the t_{exp} were in all cases below t_{crit} at a significance level of 0.05, thus indicating that the absolute recoveries for the target analytes in saliva were statistically comparable to those found in aqueous standards. The clean-up, extraction, and preconcentration capability of the 3D-printed millifluidic sorptive device is illustrated in Fig. 5A-D. Before the SPE protocol (Fig. 5A and 5B), all of the analytes were hardly detectable due to matrix interfering effects (Fig. 5A) or low concentration levels (Fig. 5B), whereas after the SPE protocol (Fig. 5D) all of the analytes could be satisfactorily quantified. The clean-up effect of the on-line SPE protocol can be clearly observed for 4-HBA, MPB and TCS, which cannot be reliably quantified without SPE because of matrix interferences (see Fig. 5C and 5D vs 5A and 5B). The automatic method was further applied to the analysis of human saliva samples of two volunteers after using a mouthwash containing TCS (see SI for more information). The proposed method allowed the quantitative determination of TCS in the two samples (134 ± 4 μg g^{-1} and 127 ± 2 μg g^{-1}), thus demonstrating the feasibility of the 3D

420 printed platform hyphenated to HPLC for reliable analysis of biological fluids with sufficient
421 sensitivity for the target species.
422

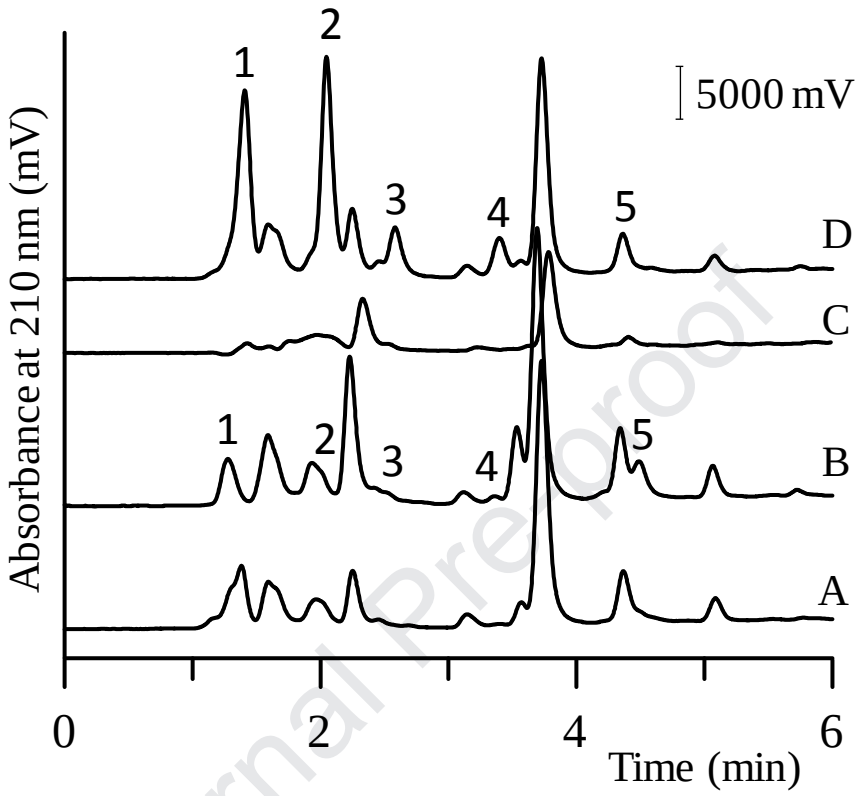

423

424 **Fig. 5.** Experimental chromatograms of direct injection of blank saliva without SPE (A), saliva
425 spiked at 250 μg L^{-1} without SPE (B), blank saliva after the on-line SPE and separation
426 methodology (C) and saliva spiked at 250 μg L^{-1} after the on-line SPE and separation
427 methodology (D). SPE conditions are given in the experimental section, whereas
428 chromatographic conditions are listed in Table S2. Peak identification: 4-HBA (1), MPB (2), BPA
429 (3), PhPB (4) and TCS (5).
430

431 **4. CONCLUSIONS**

432 This paper demonstrates for the first time the feasibility of 3D stereolithographic printing for
433 fast prototyping of supports that enable covalent immobilization of porous polymer monoliths
434 aimed at on-line sorptive microscale extraction. Ten 3D-printed columns could be fabricated

simultaneously by SLA in 3h 15 min with an estimated cost of 0.45 € each and a total liquid resin volume of 25 mL.

Several synthetic routes have been comprehensively investigated to allow 3D printed column containing fluidic devices tolerating pressure-driven flow using flow injection systems without jeopardizing the chemical stability of the monolithic phase. Besides circumventing pressure drop effects, the 3D printed monolithic phases, and particularly those decorated with AuNPs, proved to be robust and reliable for the automatic clean-up and preconcentration of antimicrobials and preservatives with varying physico-chemical characteristics with excellent absolute recoveries, loading capacities and breakthrough volumes for the tested analytes (4-HBA, MPB, BPA, PhPB and TCS). Hyphenation of the millifluidic sample processing setup to on-line HPLC separation and detection was also demonstrated by fully automatic assays of the above-mentioned personal care products in saliva samples with recoveries akin to those obtained with water.

Current research is underway in our laboratories to further expand the applicability of the 3D printed covalently attached polymer monolith devices for on-line affinity chromatographic separation of several emerging contaminants in biological specimens and high matrix environmental samples.

Acknowledgements

Manuel Miró and David J Cocovi-Solberg acknowledge financial support from the Spanish Ministry of Science, Innovation and Universities (MCIU) and the Spanish State Research Agency (AEI) through project CTM2017-84763-C3-3-R (MCIU/AEI/FEDER, EU). Enrique Javier Carrasco-Correa, José Manuel Herrero-Martínez and Ernesto Francisco Simó-Alfonso gratefully acknowledge the financial support from PROMETEO/2016/145 (Consellería de Educación, Investigación, Cultura y Deporte, Generalitat Valenciana, Spain) and RTI2018-095536-B-I00

461 (MCIU). Enrique Javier Carrasco-Correa also thanks the Generalitat Valenciana for a VALi+D
462 postdoctoral research contract (APOSTD/2019/141). The authors extend their appreciation to
463 MCIU for granting the Spanish Network of Excellence in Sample preparation (RED2018-102522-
464 T). Manuel Miró dedicates this work to Prof. Purnendu (Sandy) Dasgupta on occasion of his
465 70th anniversary for his mentorship throughout the years.

466

467 **Table 1.** Repeatability and intermediate precision expressed respectively as relative standard
468 deviation (RSD) for intra- and inter-3D printed devices containing AuNP-decorated monoliths

Analyte	Intra-3D-printed device RSD (%, n=3)	Inter-3D-printed device RSD (%, n=3)	LODs (ng mL^{-1})	LOQs (ng mL^{-1})
4-HBA	3.6	4.1	1.7	5.7
MPB	2.7	4.4	0.7	2.3
BPA	3.0	3.3	0.6	2.0
PhPB	2.9	8.2	0.6	2.0
TCS	1.4	3.8	1.6	5.3

469

470

471 **Table 2.** Absolute recoveries for the target analytes in Milli-Q water and in saliva after the
472 automatic SPE procedure with on-line detection

Analyte	Absolute recovery (%)		t_{exp}
	In water	In Saliva	
4-HBA	72.6 ± 1.3	71.3 ± 1.9	0.38
MPB	75.3 ± 1.8	77.3 ± 2.1	0.27
BPA	79.3 ± 1.7	77.5 ± 1.4	0.24
PhPB	92.2 ± 2.3	89.3 ± 2.0	0.17
TCS	88.9 ± 1.8	86.6 ± 1.7	0.18

473 The critical *t* value is 2.77 (n=6, α=0.05)

474

475

476 **FIGURE CAPTIONS**

477 **Fig. 1.** Scheme of the sequential chemical modifications of the inner surface of acrylate-based
478 3D-prints prior to *in-situ* monolith preparation. The reagents used for the modification of the
479 inner surface of the 3D printed support are: EDC: 1-Ethyl-3-(3-
480 dimethylaminopropyl)carbodiimide; NHS: N-hydrosuccinimide ;HMD: hexamethylenediamine
481 and GMA: glycidyl methacrylate.

482 **Fig. 2**. Scheme of the flow setup integrating the 3D printed AuNP-decorated covalently
483 immobilized monolithic structure as a front-end to HPLC separations.

484 **Fig. 3.** SEM micrographs of the organic monolithic covalently attached to 3D-printed fluidic
485 devices. SEM micrograph at 2000× of the parent monolithic material along the wall zone (A)
486 and parent monolithic morphology at 5000× (B).

487 **Fig. 4.** Breakdown of the loaded mass of target analytes onto the different monolithic phases
488 attached to the 3D-printed millifluidic devices for automatic SPE. The maximum absolute
489 recovery was achieved for a total elution volume of 400 µL with off-line detection. Error bars
490 are given as SD values for three extractions performed with the same 3D-printed device.

491 **Fig. 5.** Experimental chromatograms of direct injection of blank saliva without SPE (A), saliva
492 spiked at 250 µg L^{-1} without SPE (B), blank saliva after the on-line SPE and separation
493 methodology (C) and saliva spiked at 250 µg L^{-1} after the on-line SPE and separation
494 methodology (D). SPE conditions are given in the experimental section, whereas
495 chromatographic conditions are listed in Table S2. Peak identification: 4-HBA (1), MPB (2), BPA
496 (3), PhPB (4) and TCS (5).

497

498

499

500

501

REFERENCES

[1] J. Urban, Current trends in the development of porous polymer monoliths for the separation of small molecules, J. Sep. Sci. 39 (2016) 51–68. https://doi.org/10.1002/jssc.201501011.

[2] F. Svec, Y. Lv, Advances and recent trends in the field of monolithic columns for chromatography, Anal. Chem. 87 (2015) 250–273. https://doi.org/10.1021/ac504059c.

[3] E.J. Carrasco-Correa, M. Vergara-Barberán, E.F. Simó-Alfonso, J.M. Herrero-Martínez, Smart materials for solid-phase extraction applications, in: Handb. Smart Mater. Anal. Chem., John Wiley & Sons, Ltd, 2019: pp. 531–580. https://doi.org/10.1002/9781119422587.ch17.

[4] B. Fresco-Cala, S. Cárdenas, Potential of nanoparticle-based hybrid monoliths as sorbents in microextraction techniques, Anal. Chim. Acta. 1031 (2018) 15–27. https://doi.org/10.1016/j.aca.2018.05.069.

[5] F. Maya, B. Paull, Recent strategies to enhance the performance of polymer monoliths for analytical separations, J. Sep. Sci. 42 (2019) 1564–1576. https://doi.org/10.1002/jssc.201801126.

[6] D. Sýkora, V. Kašička, I. Mikšík, P. Řezanka, K. Záruba, P. Matějka, V. Král, Application of gold nanoparticles in separation sciences, J. Sep. Sci. 33 (2010) 372–387. https://doi.org/10.1002/jssc.200900677.

[7] M. Vergara-Barberán, M.J. Lerma-García, E.F. Simó-Alfonso, J.M. Herrero-Martínez, Solid-phase extraction based on ground methacrylate monolith modified with gold nanoparticles for isolation of proteins, Anal. Chim. Acta. 917 (2016) 37–43. https://doi.org/10.1016/j.aca.2016.02.043.

[8] M. Vergara-Barberán, M.J. Lerma-García, E.F. Simó-Alfonso, J.M. Herrero-Martínez, Polymeric sorbents modified with gold and silver nanoparticles for solid-phase extraction of proteins followed by MALDI-TOF analysis, Microchim. Acta. 184 (2017)

1683–1690. https://doi.org/10.1007/s00604-017-2168-5.

[9] Y. Xu, Q. Cao, F. Svec, J.M.J. Fréchet, Porous polymer monolithic column with surface-bound gold nanoparticles for the capture and separation of cysteine-containing peptides, Anal. Chem. 82 (2010) 3352–3358. https://doi.org/10.1021/ac1002646.

[10] A.Z. Zhang, F.G. Ye, J.Y. Lu, Z. Wei, Y. Peng, S.L. Zhao, Preparation and characterization of polymer solid-phase microextraction monolith modified with gold nanoparticles, Fenxi Huaxue/ Chinese J. Anal. Chem. 39 (2011) 1247–1250. https://doi.org/10.1016/S1872-2040(10)60464-1.

[11] H. Wang, H. Zhang, Y. Lv, F. Svec, T. Tan, Polymer monoliths with chelating functionalities for solid phase extraction of metal ions from water, J. Chromatogr. A. 1343 (2014) 128–134. https://doi.org/10.1016/j.chroma.2014.03.072.

[12] E.H. Hansen, M. Miró, How flow-injection analysis (FIA) over the past 25 years has changed our way of performing chemical analyses, TrAC - Trends Anal. Chem. 26 (2007) 18–26. https://doi.org/10.1016/j.trac.2006.07.010.

[13] L. Xu, Z.G. Shi, Y.Q. Feng, Porous monoliths: Sorbents for miniaturized extraction in biological analysis, Anal. Bioanal. Chem. 399 (2011) 3345–3357. https://doi.org/10.1007/s00216-010-4190-x.

[14] V. Augustin, G. Proczek, J. Dugay, S. Descroix, M.C. Hennion, Online preconcentration using monoliths in electrochromatography capillary format and microchips, J. Sep. Sci. 30 (2007) 2858–2865. https://doi.org/10.1002/jssc.200700387.

[15] M. Vázquez, B. Paull, Review on recent and advanced applications of monoliths and related porous polymer gels in micro-fluidic devices, Anal. Chim. Acta. 668 (2010) 100–113. https://doi.org/10.1016/j.aca.2010.04.033.

[16] E.K. Parker, A. V. Nielsen, M.J. Beauchamp, H.M. Almughamsi, J.B. Nielsen, M. Sonker, H. Gong, G.P. Nordin, A.T. Woolley, 3D printed microfluidic devices with immunoaffinity monoliths for extraction of preterm birth biomarkers, Anal. Bioanal. Chem. (2018).

554 https://doi.org/10.1007/s00216-018-1440-9.

555 [17] D.J. Cocovi-Solberg, P.J.P.J. Worsfold, M. Miró, Opportunities for 3D printed millifluidic
556 platforms incorporating on-line sample handling and separation, TrAC - Trends Anal.
557 Chem. 108 (2018) 13–22. https://doi.org/10.1016/j.trac.2018.08.007.

558 [18] N.P. Macdonald, J.M. Cabot, P. Smejkal, R.M. Guijt, B. Paull, M.C. Breadmore,
559 Comparing microfluidic performance of three-dimensional (3D) printing platforms,
560 Anal. Chem. 89 (2017) 3858–3866. https://doi.org/10.1021/acs.analchem.7b00136.

561 [19] A.K. Au, W. Huynh, L.F. Horowitz, A. Folch, 3D-printed microfluidics, Angew. Chem. Int.
562 Ed. 55 (2016) 3862–3881.

563 [20] B. Gross, S.Y. Lockwood, D.M. Spence, Recent advances in analytical chemistry by 3D
564 printing, Anal. Chem. 89 (2017) 57–70. https://doi.org/10.1021/acs.analchem.6b04344.

565 [21] S. Waheed, J.M. Cabot, N.P. Macdonald, T. Lewis, R.M. Guijt, B. Paull, M.C. Breadmore,
566 3D printed microfluidic devices: enablers and barriers, Lab Chip. 16 (2016) 1993–2013.
567 https://doi.org/10.1039/c6lc00284f.

568 [22] F. Li, N.P. Macdonald, R.M. Guijt, M.C. Breadmore, Increasing the functionalities of 3D
569 printed microchemical devices by single material, multimaterial, and print-pause-print
570 3D printing, Lab Chip. 19 (2019) 35–49. https://doi.org/10.1039/c8lc00826d.

571 [23] A.J. Capel, R.P. Rimington, M.P. Lewis, S.D.R. Christie, 3D printing for chemical,
572 pharmaceutical and biological applications, Nat. Rev. Chem. 2 (2018) 422–436.
573 https://doi.org/10.1038/s41570-018-0058-y.

574 [24] V. Gupta, P. Nesterenko, B. Paull, 3D Printing in Chemical Sciences, The Royal Society of
575 Chemistry, 2019. https://doi.org/10.1039/9781788015745.

576 [25] H. Wang, D.J. Cocovi-Solberg, B. Hu, M. Miró, 3D-Printed microflow injection analysis
577 platform for online magnetic nanoparticle sorptive extraction of antimicrobials in
578 biological specimens as a front end to liquid chromatographic assays, Anal. Chem. 89
579 (2017) 12541–12549. https://doi.org/10.1021/acs.analchem.7b03767.

[26] É.M. Kataoka, R.C. Murer, J.M. Santos, R.M. Carvalho, M.N. Eberlin, F. Augusto, R.J. Poppi, A.L. Gobbi, L.W. Hantao, Simple, Expendable, 3D-printed microfluidic systems for sample preparation of petroleum, Anal. Chem. 89 (2017) 3460–3467. https://doi.org/10.1021/acs.analchem.6b04413.

[27] D.J. Cocovi-Solberg, M. Rosende, M. Michalec, M. Miró, 3D Printing: the second dawn of lab-on-valve fluidic platforms for automatic (bio)chemical assays, Anal. Chem. 91 (2019) 1140–1149. https://doi.org/10.1021/acs.analchem.8b04900.

[28] C.-K. Su, P.-J. Peng, Y.-C. Sun, Fully 3D-printed preconcentrator for selective extraction of trace elements in seawater, Anal. Chem. 87 (2015) 6945–6950. https://doi.org/10.1021/acs.analchem.5b01599.

[29] W. Lee, D. Kwon, W. Choi, G.Y. Jung, A.K. Au, A. Folch, S. Jeon, 3D-Printed micro fluidic device for the detection of pathogenic bacteria using size-based separation in helical channel with trapezoid cross-section, Sci. Rep. 5 (2015). https://doi.org/10.1038/srep07717.

[30] E. Mattio, N. Ollivier, F. Robert-Peillard, R. Di Rocco, C. Branger, A. Margaillan, C. Brach-Papa, J. Knoery, D. Bonne, J.L. Boudenne, B. Coulomb, Modified 3D-printed device for mercury determination in waters, Anal. Chim. Acta. (2019). https://doi.org/10.1016/j.aca.2019.06.062.

[31] S. Sandron, B. Heery, V. Gupta, D.A. Collins, E.P. Nesterenko, P.N. Nesterenko, M. Talebi, S. Beirne, F. Thompson, G.G. Wallace, D. Brabazon, B. Paull, 3D Printed metal columns for capillary liquid chromatography, Analyst. 139 (2014) 6343–6347. https://doi.org/10.1039/c4an01476f.

[32] V. Gupta, M. Talebi, J. Deverell, S. Sandron, P.N. Nesterenko, B. Heery, F. Thompson, S. Beirne, G.G. Wallace, B. Paull, 3D Printed titanium micro-bore columns containing polymer monoliths for reversed-phase liquid chromatography, Anal. Chim. Acta. 910 (2016) 84–94. https://doi.org/10.1016/j.aca.2016.01.012.

606 [33] V. Gupta, S. Beirne, P.N. Nesterenko, B. Paull, Investigating the effect of column
607 geometry on separation efficiency using 3D printed liquid chromatographic columns
608 containing polymer monolithic phases, Anal. Chem. 90 (2018) 1186–1194.
609 https://doi.org/10.1021/acs.analchem.7b03778.
610 [34] L. Picard, P. Phalip, E. Fleury, F. Ganachaud, Chemical adhesion of silicone elastomers
611 on primed metal surfaces: A comprehensive survey of open and patent literatures,
612 Prog. Org. Coatings. 80 (2015) 120–141.
613 https://doi.org/10.1016/j.porgcoat.2014.11.022.
614 [35] E.Y. Liu, S. Jung, H. Yi, Improved Protein Conjugation with Uniform, Macroporous
615 Poly(acrylamide-co-acrylic acid) Hydrogel Microspheres via EDC/NHS Chemistry,
616 Langmuir. 32 (2016) 11043–11054. https://doi.org/10.1021/acs.langmuir.6b02591.
617 [36] C. Wang, Q. Yan, H.B. Liu, X.H. Zhou, S.J. Xiao, Different EDC/NHS activation
618 mechanisms between PAA and PMAA brushes and the following amidation reactions,
619 Langmuir. 27 (2011) 12058–12068. https://doi.org/10.1021/la202267p.
620 [37] N. Chopin, X. Guillory, P. Weiss, J.L.B. and S. Colliec-Jouault, Design Polysaccharides of
621 Marine Origin: Chemical Modifications to Reach Advanced Versatile Compounds, Curr.
622 Org. Chem. 18 (2014) 867–895.
623 https://doi.org/http://dx.doi.org/10.2174/1385272818071405151523334.
624 [38] M. Catalá-Icardo, S. Torres-Cartas, S. Meseguer-Lloret, E.F. Simó-Alfonso, J.M. Herrero-
625 Martínez, Photografted fluoropolymers as novel chromatographic supports for
626 polymeric monolithic stationary phases, Talanta. 187 (2018) 216–222.
627 https://doi.org/10.1016/j.talanta.2018.05.026.
628 [39] E.J. Carrasco-Correa, G. Ramis-Ramos, J.M. Herrero-Martínez, Hybrid methacrylate
629 monolithic columns containing magnetic nanoparticles for capillary
630 electrochromatography, J. Chromatogr. A. 1385 (2015).
631 https://doi.org/10.1016/j.chroma.2015.01.044.

[40] D.J. Cocovi-Solberg, M. Miró, CocoSoft: educational software for automation in the analytical chemistry laboratory, Anal. Bioanal. Chem. 407 (2015) 6227–6233. https://doi.org/10.1007/s00216-015-8834-8.

[41] E. Javier Carrasco-Correa, P. Kubáň, D.J. Cocovi-Solberg, M. Miró, Fully automated electric-field-driven liquid phase microextraction system with renewable organic membrane as a front end to high performance liquid chromatography, Anal. Chem. 91 (2019) 10808–10815. https://doi.org/10.1021/acs.analchem.9b02453.

[42] E.J. Carrasco-Correa, G. Ramis-Ramos, J.M. Herrero-Martínez, Evaluation of 2,3-epoxypropyl groups and functionalization yield in glycidyl methacrylate monoliths using gas chromatography, J. Chromatogr. A. 1379 (2015). https://doi.org/10.1016/j.chroma.2014.12.050.

[43] D. Aureau, Y. Varin, K. Roodenko, O. Seitz, O. Pluchery, Y.J. Chabal, Controlled deposition of gold nanoparticles on well-defined organic monolayer grafted on silicon surfaces, J. Phys. Chem. C. 114 (2010) 14180–14186. https://doi.org/10.1021/jp104183m.

[44] C. André, Y.C. Guillaume, Boron nitride nanotubes and their functionalization via quinuclidine-3-thiol with gold nanoparticles for the development and enhancement of the HPLC performance of HPLC monolithic columns, Talanta. 93 (2012) 274–278. https://doi.org/10.1016/j.talanta.2012.02.033.

[45] T. Khezeli, A. Daneshfar, Monodisperse silica nanoparticles coated with gold nanoparticles as a sorbent for the extraction of phenol and dihydroxybenzenes from water samples based on dispersive micro-solid-phase extraction: Response surface methodology, J. Sep. Sci. 38 (2015) 2804–2812. https://doi.org/10.1002/jssc.201500320.

[46] A. Mehdinia, E. Khojasteh, T. Baradaran Kayyal, A. Jabbari, Magnetic solid phase extraction using gold immobilized magnetic mesoporous silica nanoparticles coupled

with dispersive liquid-liquid microextraction for determination of polycyclic aromatic hydrocarbons, J. Chromatogr. A. 1364 (2014) 20–27. https://doi.org/10.1016/j.chroma.2014.08.063.

[47] M. Catalá-Icardo, C. Gómez-Benito, E.F. Simó-Alfonso, J.M. Herrero-Martínez, Determination of azoxystrobin and chlorothalonil using a methacrylate-based polymer modified with gold nanoparticles as solid-phase extraction sorbent, Anal. Bioanal. Chem. 409 (2017) 243–250. https://doi.org/10.1007/s00216-016-9993-y.

[48] D.D. Sewu, P. Boakye, S.H. Woo, Highly efficient adsorption of cationic dye by biochar produced with Korean cabbage waste, Bioresour. Technol. 224 (2017) 206–213. https://doi.org/10.1016/j.biortech.2016.11.009.

Highlights

Organic monoliths are for the first time covalently attached to non-metallic 3D printed columns

Hydrolytic cleavage is circumvented

Integration of the monolithic column in a fully automatic millifluidic device for SPE

On-line preconcentration and clean-up of emerging contaminants in biological samples

Credit Author Statement

Enrique Carrasco-Correa: Conceptualization; Investigation; Methodology; Validation; Visualization; Formal Analysis; Roles/Writing-original draft

David J. Cocovi-Solberg: Software; Data curation

José Manuel Herrero-Martínez: Supervision; Funding acquisition; Writing - review & editing

Ernesto Simó-Afonso: Supervision; Funding acquisition; Writing - review & editing

Manuel Miró: Conceptualization; Methodology; Supervision; Funding acquisition; Project administration; resources; Writing - review & editing

Declaration of Interest Statement

The authors declared that they do not have any commercial or associative interest that represents a conflict of interest in connection with the manuscript submitted.